Avrupa Bilim ve Teknoloji Dergisi
Özel Sayı 22, S. 49-59, Ocak 2021

Derleme Makalesi

www.ejosat.com ISSN:2148-2683

European Journal of Science and Technology
Special Issue 22, pp. 49-59, January 2021

Review Article

Combustion Characteristics and Soot Formation of Shale Gases

Mehmet Salih Cellek

Bingöl Üniversitesi, Mühendislik ve Mimarlık Fakültesi, Makine Mühendisliği Bölümü, Bingöl, Türkiye, (ORCID: 0000-0001-5802-0715), mscellek@bingol.edu.tr

(First received December 2020 and in final form January 2021)

(**DOI:** 10.31590/ejosat.839848)

ATIF/REFERENCE: Cellek, M.S. (2021). Combustion Characteristics and Soot Formation of Shale Gases. *European Journal of Science and Technology*, (22), 49-59.

Abstract

In this study, non-premixed combustion characteristics and soot formation of methane and various shale gaseous have been investigated in a combustion chamber under lean combustion conditions. After validation of the soot model with published experimental data, the flame characteristics considering flame lengths and diameters, intermediate species, temperatures, and pollutants of shale gaseous have been compared. The findings of this study show that the Moss-Brookes soot model predicts more accurate than the One-Step and Method of Moments models. Since the Methods of Moment method estimates higher soot formation than the experimental method, while the One-Step method estimates lower. The flame characteristics show that although the flame temperatures are close to each other, they differ relatively. In addition, flame lengths, flame reaction zones, and intermediate product concentrations differ similarly, and these differences also emerge as a factor in soot formation. Furthermore, the highest amount of soot is released during the combustion of Barnett shale gas. It is minimal for methane despite emitting intermediate species as much as shale gases. Since more unburned C elements released during the combustion of shale gases. Therefore, when the C/H ratio in hydrocarbon fuels increases, the amount of soot emitted from the flame also increases.

Keywords: Shale gas, Soot, Soot formation, Moss-Brookes.

Kaya Gazlarının Yanma Karakteristikleri ve İs Oluşumu

Öz

Bu çalışmada, fakir karışım koşullarında bir yanma odasında metan ve farklı bileşenlere sahip çeşitli kaya gazlarının difüzyon alevleri ve kurum oluşumları incelenmiştir. Kurum modelinin yayınlanmış deneysel verilerle doğrulanmasından sonra, kaya gazlarının alev uzunlukları ve çapları, ara ürünleri, sıcaklıklar ve kirleticiler dikkate alınarak alev karakteristikleri karşılaştırılmıştır. Bu çalışmanın bulgularına göre, Moss-Brookes kurum modelinin One-Step ve Method of Moments modellerine göre daha doğru tahminlerde bulunduğu görülmektedir. Çünkü Methods of Moment yöntemi deneysel yönteme göre yüksek kurum tahmini yapmakta, One-Step yöntemi ise daha düşük tahminde bulunmaktadır. Alev karakteristikleri göstermektedir ki alev sıcaklıkları birbirine yakın olmasına rağmen, göreceli de olsa farklılık göstermektedir. Ayrıca alev uzunlukları, alev reaksiyon bölgeleri ve ara ürün konsantrasyonlarıda benzer şekilde farklılıklar göstermekte, bu farklılıklar da is oluşumu üzerinde birer etken olarak ortaya çıkmaktadır. Dahası Barnett kaya gazı yanma sırasında en yüksek miktarda kurum yaymaktayken, kaya gazları kadar ara ürün yaymasına rağmen metan gazı en az kurum yaymaktadır. Çünkü kaya gazlarının yanması sırasında daha fazla yanmamış C elementi açığa çıkmaktadır. Bu nedenle, hidrokarbon yakıtlarda C/H oranı arttığında, alevden yayılan kurum miktarı da artar.

Anahtar Kelimeler: Kaya gazı, is, is oluşumu, Moss-Brookes.

1. Introduction

Shale gas is a type of natural gas captured within shale formations. Since the beginning of the 2000s, it has gained importance in the USA and its importance has increased in proportion to the amount extracted in the following years. Less than 1% of the natural gas production was obtained with shale gas in 2000. Then, it rose over 20% by 2010 and it will reach 46% of US natural gas by 2035 according to point of view of the US government's Energy Information Administration (Stevens, P., 2012). Because the cost of extraction is higher than traditional natural gas, a few countries follow the United States as China, India, Poland, South Africa, Australia, UK, and Ukraine (Ozturk, 2019). Nevertheless, due to the increase in demand for energy resources, these countries are expected to increase their interest in shale gas in the coming years.

According to the research published by U.S. Energy Information Administration (EIA, 2015), Turkey has two prospective basins of shale gas specifically SE Anotolia and Thrace basins. In addition to these, they stated that there may be two different basins such as Salt Lake and Sivas basins, which are not finalized due to limited reservoir data for these two lightly explored basins. They also told that the shale gas located in the average 2743-2895 m and 388-1761 m dept, 83148.54 -16836.93 km^2 basin/gross area for the SE Anotolia and Thrace basins, respectively. The total capacity of shale gas in Turkey for two basins is declared in the same report as 163 Tcf (≅ 4.6 trillion m^3) risked GIB, or 24 Tcf (≅ 679 billion m^3) risked recoverable. According to the Ilbas, 2017; the potential of the production of shale gas in Turkey need such a long time about ten years. It does not seem possible in the near production to Turkey. However, despite everything, R&D studies, examination, research and drilling studies, technical equipment and infrastructure studies should be continued. Although shale gas potential is not high, it should be taken into consideration that it is much higher than natural gas reserves. In another study conducted by Karsli, 2015; some difficulties related to environmental, geographic, technological, and pipeline system must be overcome in order to extract and use shale gas in Turkey. Karslı also state that a minimum period of 10 years is needed to benefit from shale gas.

The calorific values of shale gases, qualities, gas components, and the percentage of components differ from region to region. In terms of shale gas Barnett, Haynesville, and Fayetteville are popular areas in the South, New Albany, Marcellus and Antrim are in the East and Midwest in the US (Bullin, 2008).

On the other hand, the study of soot formation is of particular interest due to various factors. Black soot (industrial carbon) is a commercial product, with an annual world production of 107 tons a year, and utilized as a filler for elastomers and in copy machines and laser printers (Mansurov, 2005). Additionally, the existence of soot in a furnace and boiler raises radiation and hence the efficiency of heat transfer from the flame (Haynes and Wagner, 1981). On the other hand, it also causes some problems that have worried researchers for a long time. Smoke emissions cause to increase particulate loading of the atmosphere imply that adverse health effects, including premature death, heart attacks, and strokes, as well as acute bronchitis and aggravated asthma (Environmental Defence Fund (EDF), t.y.). Furthermore, particles deposited on the surface of leaves inhibits light penetration, increases surface temperature due to absorption of heat and clogging of stomata. These reduce gaseous exchange, photosynthesis, and plant growth (Gheorghe and Ion, 2011). As a result, in addition to greenhouse gases, which have significant effects on climate change (Gurbuz and Sandalcı, 2019; Gurbuz, 2020), soot formation also has environmental hazards.

Emissions arise from shale gas results from the energy used in the drilling of the well bore, and in the pumping of water and other material during hydraulic fracturing. The fracturing phase and drilling operation requires significantly intense energy and normally provided by large, diesel-fired internal combustion engines thay emit pollutants including CO_2 during the combustion. The quantity of fuel consumed, and pollutants will depend upon the length of the well bore (AEA, 2012).

In general, soot emission in the flue gas reveals poor combustion conditions and a loss of efficiency. Besides, the deposition of the soot in the combustion systems requires maintenance for the high efficiency of the devices. Under these circumstances, it is significant to be able to oxidize the particles before leaving the furnace. The time typically available for the formation of soot is of the order of a few milliseconds. During this time, some of the fuel is transformed to give rise to the solid soot particles (Haynes and Wagner, 1981). The resulting soot aerosol can be characterized by the total amount of the condensed phase, often expressed as the soot volume fraction q~(cm^3 soot/cm^3); the number of soot particles, N (cm-3); and the size of the particles, d (Haynes and Wagner, 1981). In short, due to the reasons stated above, we need to pay attention to soot and soot formation issues.

Although there are many studies focused on combustion of various fuels in the literature, a few ones are related to shale gas. In the numerical and experimental study of Vargas et al, 2016, the combustion characteristics of several typical shale gas mixtures including laminar burning velocities, the thickness of flame fronts, lower and higher heat values, Wobbe indices, flammability limits, dew points, and adiabatic flame temperatures investigated. On the other hand, experimental and numerical studies focused on soot formation are shown in the table below. In addition, Ozturk (2019) investigated the effects of equivalence ratio, wall temperature, fuel and oxide inlet temperatures on combustion of shales gases namely Fayetteville, New Albany, and Haynesville. He found that the NO mass fraction reached maximum value about stoichometric ecoivalance ratio. Increasing in wall temperature raises both NO and CO mass fractions.

The turbulent, non-adiabatic, and non-premixed combustion of shale gas and air in a cylindrical combustor is computationally investigated under the effects of equivalence ratio, wall temperature, fuel and oxide inlet temperatures. As a result of the investigations in the literature, no studies were found on the formation of soot during the combustion of shale gases. Therefore, in this study, combustion flames and soot formation of methane and various shale gaseous originated from Barnett, New Albany, and Haynesville have been investigated under the lean condition at 8.6 kW in a combustion chamber. The effects of gaseous species and radicals on the flames and soot formation were also discussed.

Table 1. A brief literature survey on soot formation investigation for various fuels and flames

Authors	Method	Fuel-Oxidixer	Flame Type	Soot Model
Lu et al., 2016	Exp.	Ethylene-Air	Diffusion Flame	-
Cuoci et al., 2008	CFD	Ethylene-Air Methane-air	Diffusion Flame	One-step reaction
Razak et al., 2019	Exp. CFD	N-dodecane-air	Spray Flame	Moss-Brookes
Hernandez et al., 2013	CFD	Ethylene-Air	Counterflow Diffusion flames	Leung et al. Semi-Empriacal
Watanabe et al., 2006.	CFD	N-decane-Air	Counterflow Spray flame	A kinetically based soot model
Manin et al., 2014.	Exp.	Liqued Fuels (G15, G33, G50, G50A, MD and C12) +air	Diffusion Flame	-
Lautenberger et al., 2005	CFD	Ethylene, Propylene, Propane	Diffusion Flame	A new model developed
Palazzo et al., 2019	Exp.	Diesel-air	Diffusion Flame	-
Ito et al., 2003	Exp.	Diesel-air DBE-air DGB-air DGE-air	Diffusion Flame	-
Roditcheva and Bai., 2001	CFD	Methane-air	Diffusion Flame	Semi-empirical soot model developed by Moss et al.(1988)
Xu et al., 2020.	Exp.	Coal+air	Diffusion Flame	-
Kazem et al., 2007	Exp. CFD	Kerosene+air	Diffusion Flame	Moss
Chong et al., 2019	Exp. CFD	Ethylene+air	Diffusion Flame	Semi emprical, HMOM, CQMOM

2. Material and Method

2.1. Numerical Model

Numerical combustion flame investigation of methane and shale gaseous has been carried out in a cylindrical combustion chamber based on the study published by Brookes and Mass, 1999. The fuel and air coaxially enter the combustion chamber for the same thermal load of 8.6 kW. The fuels and air temperatures are the same as 290K. The combustion is performed under the lean condition with the equivalence ratio (θ) of 0.25. Non-premix combustion with Steady Diffusion Flamelet model has used for the chemical reactions. DO radiation model has used for the radiation heat transfer. Realizable $k-\varepsilon$ turbulence model has used for the turbulent predictions. Coupled and PRESTO! have been used for the pressure-velocity coupling scheme and pressure spatial discretization, respectively. ANSYS FLUENT 18.2 (Ansys Inc, 2018).software has been used for the numerical calculations.

To study the numerical approximations of partial differential equations, the computational fluid dynamic (CFD) technique is used. In this technique, there is a wide range of numerical methodologies, algorithms, schemes, simulation strategies as well as software programs for the solution (Afshari et al., 2018). Reynolds-Averaged Navier-Stokes (RANS) equations (momentum, mass conservation (continuity), energy) which are nonlinear describes the motion of viscous, heat-conducting fluid in nature are resolved with ANSYS Fluent18.2 (Ansys Inc, 2018). The transport of the average flow quantities is governed by the RANS equations, with the whole range of turbulence scale being modeled with Spalart-Allmaras, k-ε and its variants, k-ω and its variants, and the RSM. These models are widely adopted for engineering applications, especially as they greatly reduce the required computational effort and resources (Ansys, Inc. 2009). Realizable $k-\varepsilon$ is used for the turbulence predictions.

For 2D axisymmetric geometries, the continuity equation is given by (Ansys, Inc., 2009)

$$\frac{\partial \rho}{\partial t}+\frac{\partial}{\partial x}(\rho v_x)+\frac{\partial}{\partial r}(\rho v_r)+\frac{\rho v_r}{r}=S_m \quad (1)$$

For 2D axisymmetric geometries, the axial and radial momentum conservation and energy equations are given by

$$\frac{\partial}{\partial t}(\rho v_x)+\frac{1}{r}\frac{\partial}{\partial x}(r\rho v_x v_x)+\frac{1}{r}\frac{\partial}{\partial r}(r\rho v_r v_x)=-\frac{\partial p}{\partial x}+\frac{1}{r}\frac{\partial}{\partial x}\left[r\mu\left(2\frac{\partial v_x}{\partial x}-\frac{2}{3}(\nabla\cdot\vec{v})\right)\right]+\frac{1}{r}\frac{\partial}{\partial r}\left[r\mu\left(\frac{\partial v_x}{\partial r}+\frac{\partial v_r}{\partial x}\right)\right]+F_x \quad (2)$$

$$\frac{\partial}{\partial t}(\rho v_r)+\frac{1}{r}\frac{\partial}{\partial x}(r\rho v_x v_r)+\frac{1}{r}\frac{\partial}{\partial r}(r\rho v_r v_r)=-\frac{\partial p}{\partial r}+\frac{1}{r}\frac{\partial}{\partial x}\left[r\mu\left(\frac{\partial v_r}{\partial x}+\frac{\partial v_x}{\partial r}\right)\right]+\frac{1}{r}\frac{\partial}{\partial r}\left[r\mu\left(2\frac{\partial v_r}{\partial r}-\frac{2}{3}(\nabla\cdot\vec{v})\right)\right]-2\mu\frac{v_r}{r^2}+\frac{2}{3}\frac{\mu}{r}(\nabla\cdot\vec{v})+\rho\frac{v_z^2}{r}+F_r \quad (3)$$

$$\nabla\cdot\vec{v}=\frac{\partial v_x}{\partial x}+\frac{\partial v_r}{\partial r}+\frac{v_r}{r} \quad (4)$$

$$\frac{\partial}{\partial t}(\rho E) + \nabla \cdot \left(\vec{v}(\rho E + p)\right) = \nabla \cdot \left(k_{eff} \nabla \mathrm{T} - \sum_j h_j \vec{J}_j + \left(\bar{\bar{\tau}}_{eff} . \vec{v}\right) \right) + S_h \quad (5)$$

where x and r are the axial and radial coordinates. Besides v_x, v_r, and v_z are the axial, radial, and swirl velocities, respectively. k_{eff} is the effective conductivity $(k + k_t)$, $\vec{J}_j$ is the diffusion flux of species j, the first three terms on the right-hand side of Equation 5 represent energy transfer due to conduction, species diffusion, and viscous dissipation, respectively. The last term S_h, includes the heat of chemical reactions and any other volumetric heat sources (Ansys, Inc. 2009).

2.1.1. Soot Formation Models

Moss-Brookes Soot Model

Transport equations for normalized radical nuclei concentration b^*_{nuc} and soot mass fraction Y_{soot} is calculated by Moss-Brookes model (Ansys, Inc., 2009).

$$\frac{\partial}{\partial t}(\rho Y_{soot}) + \nabla \cdot (\rho \vec{v} Y_{soot}) = \nabla \cdot \left(\frac{\mu_t}{\sigma_{soot}} \nabla Y_{soot} \right) + \frac{dM}{dt} \quad (6)$$

$$\frac{\partial}{\partial t}(\rho b^*_{nuc}) + \nabla \cdot (\rho \vec{v} b^*_{nuc}) = \nabla \cdot \left(\frac{\mu_t}{\sigma_{nuc}} \nabla b^*_{nuc} \right) + \frac{1}{N_{norm}} \frac{dN}{dt} \quad (7)$$

where Y_{soot} is the soot mass fraction, M is the soot mass concentration (kg/m^3), b^*_{nuc} is normalized radical nuclei concentration (particles$\times 10^{-15}$/kg) $= \frac{N}{\rho N_{norm}}$, N is the soot particle number density (particles/m^3), N_{norm} corresponds 10^{15} particles. The production rate of soot particles in the free molecular regime is given by (Ansys, Inc., 2009).

$$\frac{dN}{dt} = C_\alpha N_A \left(\frac{X_{prec} P}{RT} \right)^l exp\left(-\frac{T_\alpha}{T} \right) - C_\beta \left(\frac{24RT}{\rho_{soot} N_A} \right)^{\frac{1}{2}} d_p^{\frac{1}{2}} N^2 \quad (8)$$

where C_α, C_β, l are model constants. N_A is the Avogadro number, X_{prec} is the mole fraction of soot precursor namely acetylene for studied fuels. Density of soot, ρ_{soot}, equals to 1800 kg/m^3 and d_p is the mean diameter of a soot particle. The first term of the right side equation corresponds nucleation and the second refers coagulation (Ansys, Inc., 2009).

$$\frac{dM}{dt} = M_P C_\alpha \left(\frac{X_{prec} P}{RT} \right)^l exp\left(-\frac{T_\alpha}{T} \right) - C_\gamma \left(\frac{X_{sgs} P}{RT} \right)^m exp\left(-\frac{T_\gamma}{T} \right) \left[(\pi N)^{\frac{1}{3}} \left(\frac{6M}{\rho_{soot}} \right)^{\frac{2}{3}} \right]^n - C_{oxid} C_w \eta_{coll} \left(\frac{X_{OH} P}{RT} \right) \sqrt{T} (\pi N)^{\frac{1}{3}} \left(\frac{6M}{\rho_{soot}} \right)^{\frac{2}{3}} \quad (9)$$

where the first term of the right side equation corresponds to nucleation, the second term of the equations corresponds to the surface growth, and the last term of the right side equation refers to oxidation. The constant M_p is the mass of incipient soot particles. X_{sgs} is the mole fraction of the participating surface growth species. Assuming a collision efficiency (η_{coll}) of 0.004. The constant values for the C_α, T_α, C_β, C_γ, T_γ, C_w, C_{oxid} are 54 s^{-1}, 21000 K, 1.0, 11700 kg.m.kmol^{-1}. s^{-1}, 121000 K, 105.8125 kg.m.kmol^{-1} . K$^{-1/2}$. s^{-1}, and 0.015, respectively (Ansys, Inc., 2009).

One-Step and Method of Moments Soot Models

In the One-step (Khan and Greeves, 1974) model, a single transport equation is solved for the soot mass fraction. The rate of soot combustion is the minimum of two rate expressions $\mathrm{R_{soot,comb}} = \min [\mathrm{R_1}, \mathrm{R_2}]$ (Ansys, Inc., 2009).

$$R_1 = A \rho Y_{soot} \frac{\varepsilon}{k} \quad (10)$$

$$R_2 = A \rho \left(\frac{Y_{ox}}{v_{soot}} \right) \left(\frac{Y_{soot} v_{soot}}{Y_{soot} v_{soot} + Y_{fuel} v_{fuel}} \right) \frac{\varepsilon}{k} \quad (11)$$

Where A is the Magnussen model, Y_{ox}, Y_{fuel} are mass fractions of oxidizer and fuel, v_{soot} and v_{fuel} are mass stoichiometries for soot and fuel combustion. The one-step model constants are valid for numerous hydrocarbon fuels (Ansys, Inc., 2009).

The other soot formation model namely, Method of Moments was proposed by Frenklach et al., 1987, and it depends on the transport of the moments of the NDF function. Principally, the distribution function can be reconstructed if all integer moments are available. But, in practical cases, the first few moments give enough information to obtain the sought properties of the distribution (Frenklach, 2002 and Bodor, 2019).

2.1.2. Fuel Components and Properties

In the present study, in addition to methane, various shale gaseous namely Barnett Shale Gas, New Albany, and Haynesville having different contents have simulated in the same combustion chamber. The mentioned shale gases, their components, H/C ratios as well as mass flow inlet of the simulations are presented in Table 1.

Table 1. Simulated shale gaseous (Bullin and Krouskop, 2008) with operating conditions

Components	Barnett	New Albany	Haynesville
CH_4	0.812	0.89875	0.95
C_2H_6	0.118	0.01125	0.001
C_3H_8	0.052	0.01125	-
CO_2	0.003	0.07875	0.048
N_2	0.015	-	0.001
H/C	3.633	3.940	3.998
MW. [kg/kgmol]	19.42	18.71	17.41
Hu[Mj/kg]	47.72	40.63	43.88
Pressure	1 atm	1 atm	1 atm
T_{air} *and* T_{fuel}	290 K	290 K	290 K
$\dot{m}_a$ *[kg/s]*	0.011713	0.011759	0.011769
$\dot{m}_f$ *[kg/s]*	0.000180	0.000211	0.000195

3. Results and Discussion

3.1. Verification and Validation of the Numerical Model

At the beginning of this study, combustion of methane have been analyzed with four different mesh numbers to reveal the verification of the numerical model. Thus, the results of the simulations have compared to ensure the mesh independence study. Taking into account the upper flame temperature, CO and CO_2 emissions, it has determined that 122710 cells are adequate for obtaining acceptable numerical results. Structured boundary layer grids have utilized for mesh generation as shown in Fig. 1. Therefore, enhanced wall function is utilized for the near wall modeling (Cellek, 2020).

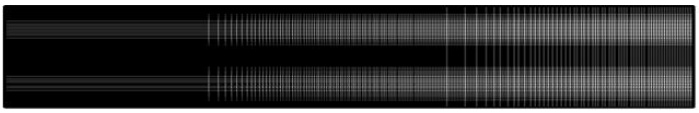

Fig.1 Mesh generation for the computational domain

Table 2. Mesh indepence study of the numerical model

Mesh Number	Tmax [K]	CO [ppm]	CO_2 [%]
42144	1794.61	0	2.66
122710	1786.58	0.68	2.69
300616	1784.34	0.69	2.68
1067680	1784.21	0.69	2.69

On the other hands, thanks to the experimental data published by Brookes and Moss, 1999, the soot formation during the methane combustion has been validated with different numerical models, namely One-step, Method of Moments, and Moss-Brookes models. Thus, soot prediction capabilities of numerical models have compared as shown in Fig. 2a-b.

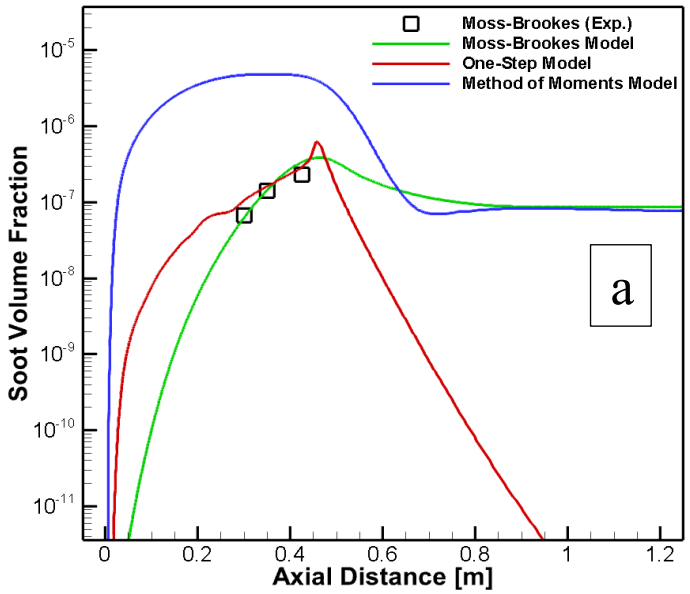

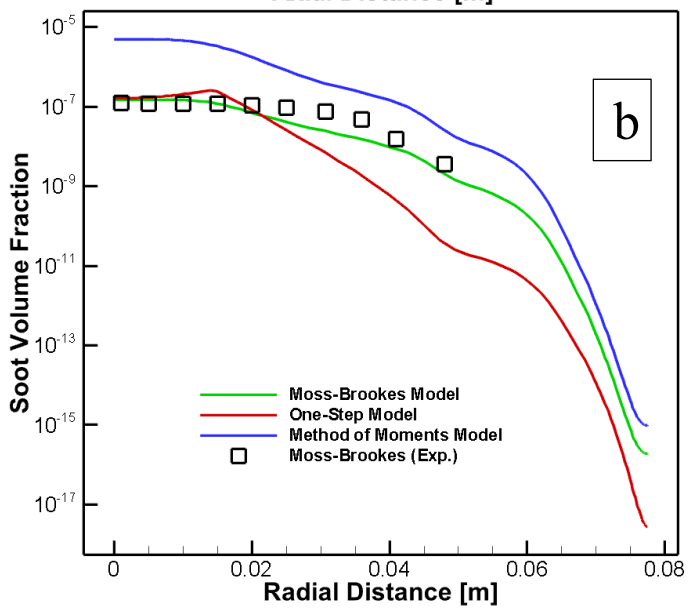

-continue

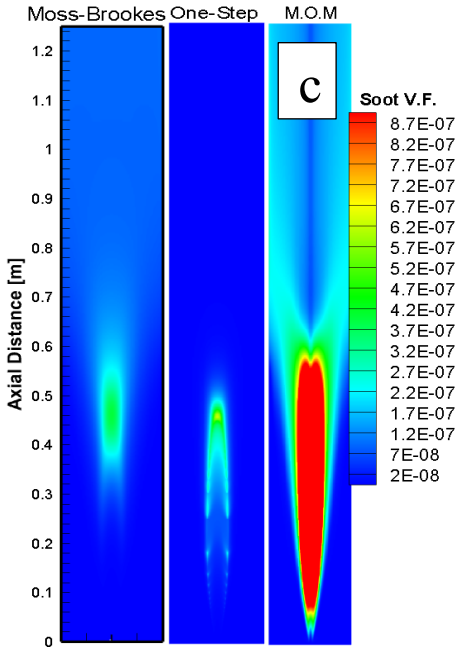

Fig. 2. Comparison of experimental and numerical results of soot volume fractions emitted from methane combustion

The obtaining soot volume fraction results on axial and radial lines show that the Moss-Brookes model predicts better than both the One-Step and Method of Moments models. Additionally, the soot volume fraction distribution on the center plane of the chamber is located in Fig. 2c. When the distribution of soot in the combustion chamber is examined, it is seen that there is excess soot in the chamber predicted with the Moments method, however, it occurs at a more reasonable level with the other two methods. In these two methods, the soot is formed gradually from the entrance and reaches its peak value at an axial distance of 0.45 m. In the One-Step method, there is a sharp decrease in the soot amount after the peak value. However, it decreases at a low speed towards the exit after the peak value using the Moss-Brookes method.

3.2. Combustion Flames of Simulated Fuels

The mass fraction distribution of CH_4 species, one of the shale gas components, along the axis of the combustion chamber is shown in Fig. 3a. In the examination, the mass fraction drops sharply from the entrance of the chamber for all gases. All of the CH_4 is consumed up to a distance of 0.65 m from the combustion chamber. On the other hand, the variation of the O_2 as a reactant species along the combustion chamber axis is also shown in Fig. 3a. The amount of oxygen in the reaction zone is minimal, while it begins to increase towards the end of the reaction zones and remains constant towards the end of the combustion chamber. Thanks to the reaction heat released during the combustion of fuels, the temperature in the combustion chamber, especially in the reaction zone, rises significantly around 0.5 m, and then a gradual decrease occurs towards the end of the reaction zone. The change of the temperature in the combustion chamber on the axis line is shown in Fig. 3b. The upper level of the flame temperatures of each fuel are close to each other and vary between 1786 -1796 K. It is approximately 860 K at the exit of each combustion chamber. While the highest flame temperature is obtained in the combustion of methane, the lowest value is obtained in New Albany shale gas combustion.

The mass fraction of OH, CH, CN, and HCN intermediates released during the combustion of shale gases are shown in Figs. 4a-d. In the investigations, these intermediate species usually occur in a certain region of the combustion chamber, especially in the reaction zone. Furthermore, they join the reaction chain and sharply decrease or turn into other types of species at the end of the reaction zone. It is seen from the distribution graphs that the released OH species levels are approximately close to each other and are effective between 0.25-0.85 m on the axis of the combustion chamber. CH intermediates species appear between 0.20-0.75 m. Besides, in terms of concentration levels in the combustion chamber, CH reaches the highest level in CH_4 and the lowest in New Albany shale gas. CN intermediates, on the other hand, occur in the same reaction zone as the CH intermediate, but in higher amounts in terms of concentration. While the CN intermediate level is high in methane and Barnett shale gas, it is relatively lower in New Albany shale gas. Finally, when the HCN intermediate concentration variation is examined, unlike other intermediates, it is formed due to the destruction of hydrocarbon fuels from the entrance of the combustion chamber, it reaches the peak level at an axial distance of 0.25 m, and then gradually decreases at the end of the reaction zone (0.75 m). During the combustion of methane and Barnett shale gas, the highest amount of HCN intermediates releases, while the lowest intermediate concentration is emitted during the combustion of New Albany shale gas.

The changes of C_2H_4 and C_2H_6 species along the axis line in the combustion chamber are shown in Fig. 5a-b. Barnett shale gas, which is one of the higher energy content due to its higher heating value (LHV) compared to other fuels, also contains higher hydrocarbon components such as C_2H_4 and C_2H_6 compared to other shale gases. The mean mixture fraction of fuel and CO species distribution are presented in Fig. 6a-b. Unburned fuel species ratio of shale gases are higher than methane. As a result of unburned fuel species, CO species of shale gases dominated in the combustion chamber.

The levels of soot released during the combustion of shale gases and methane are shown in the Fig. 7. When the results are examined, it is seen that methane has the lowest soot formation rate, on the other hand Barnett shale gas has the highest. The soot formation develops slightly at the beginning of the reaction zone and then increases sharply due to relasing effective intermediates and unsufficient O_2 concentration. With the end of the reaction zone, where soot formation reaches the peak value, the soot formation rate decreases sharply. Then the amount of the soot remains constant in the rest of chamber. The soot level in Barnett gas combustion drops slightly towards the combustion chamber exit, below the New Albany emission level. With the increase in the H/C ratio, the formation of soot in the combustion chamber decreases. In other words, as the C/H ratio in hydrocarbon fuels increases, the amount of soot increases. The levels of releasing soot inside chamber are related to unburned C species, which effects can be shown in Fig 6.

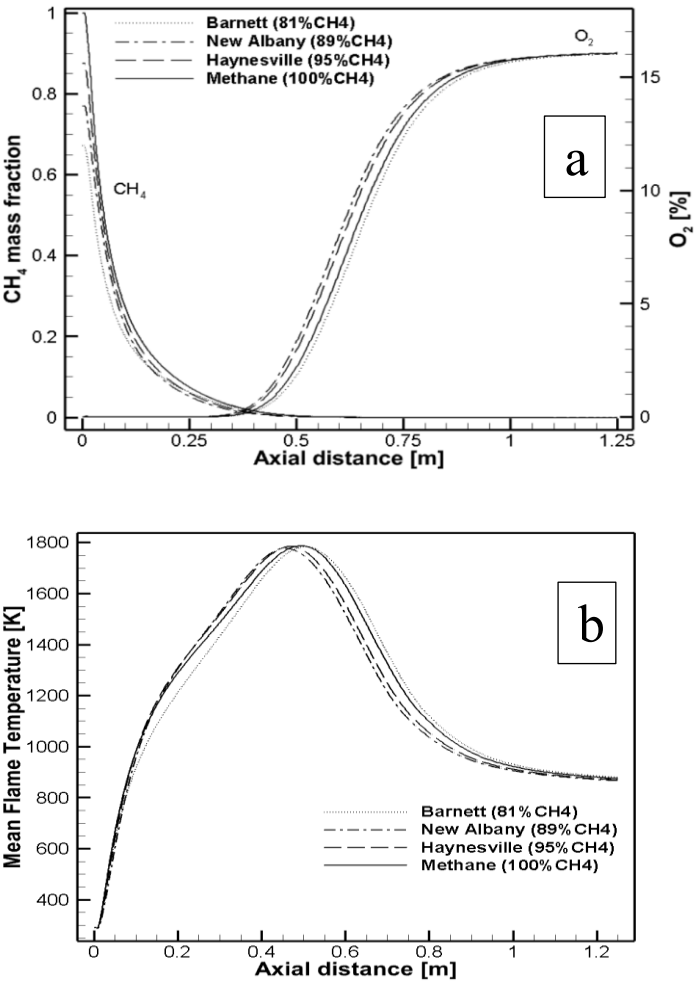

Fig. 3. Mass fraction of reactants (a) and flame temperature (b) distribution on the axial line of the chamber

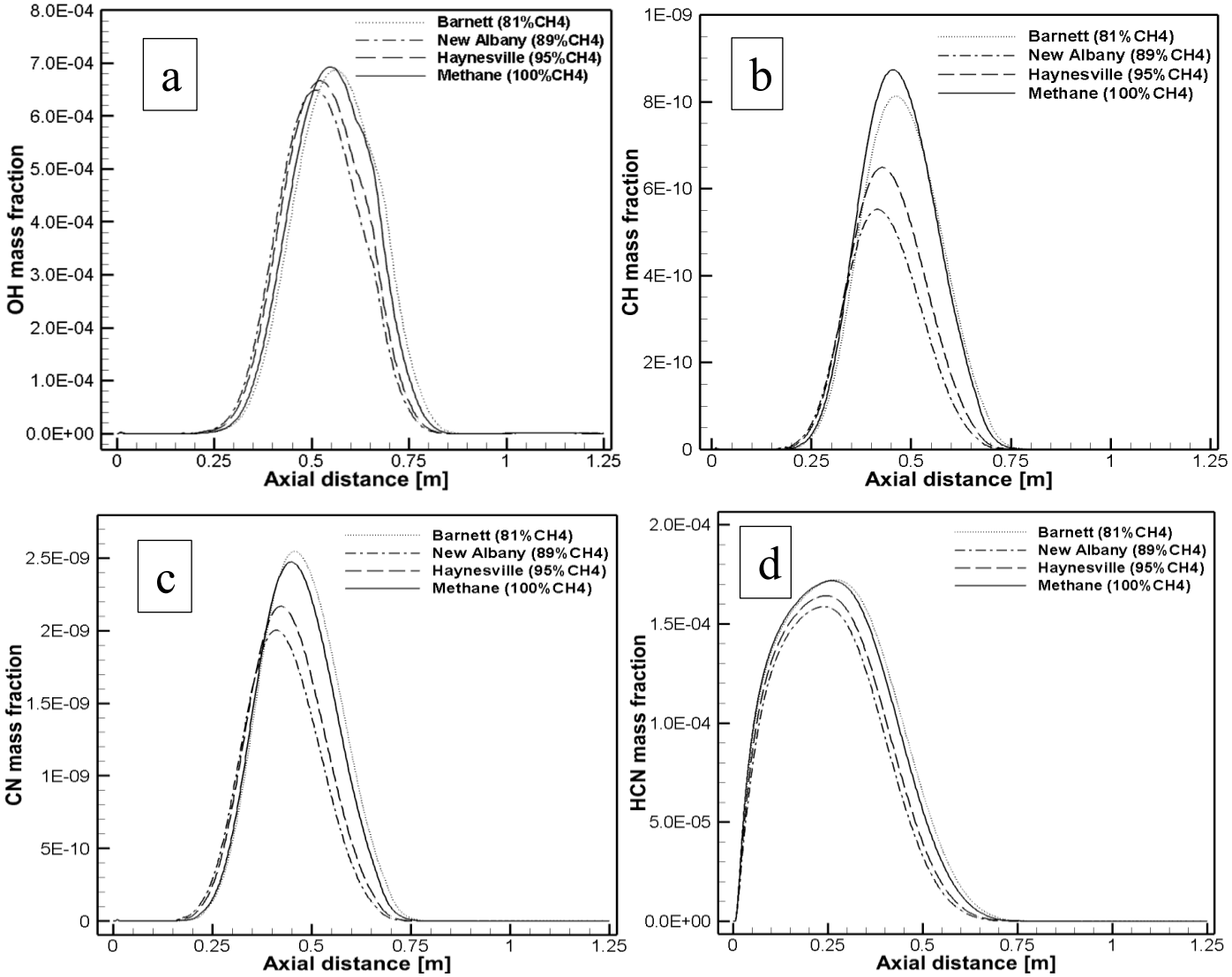

Fig. 4. The distribution of OH, CH, CN and HCN intermediate species on the axial line

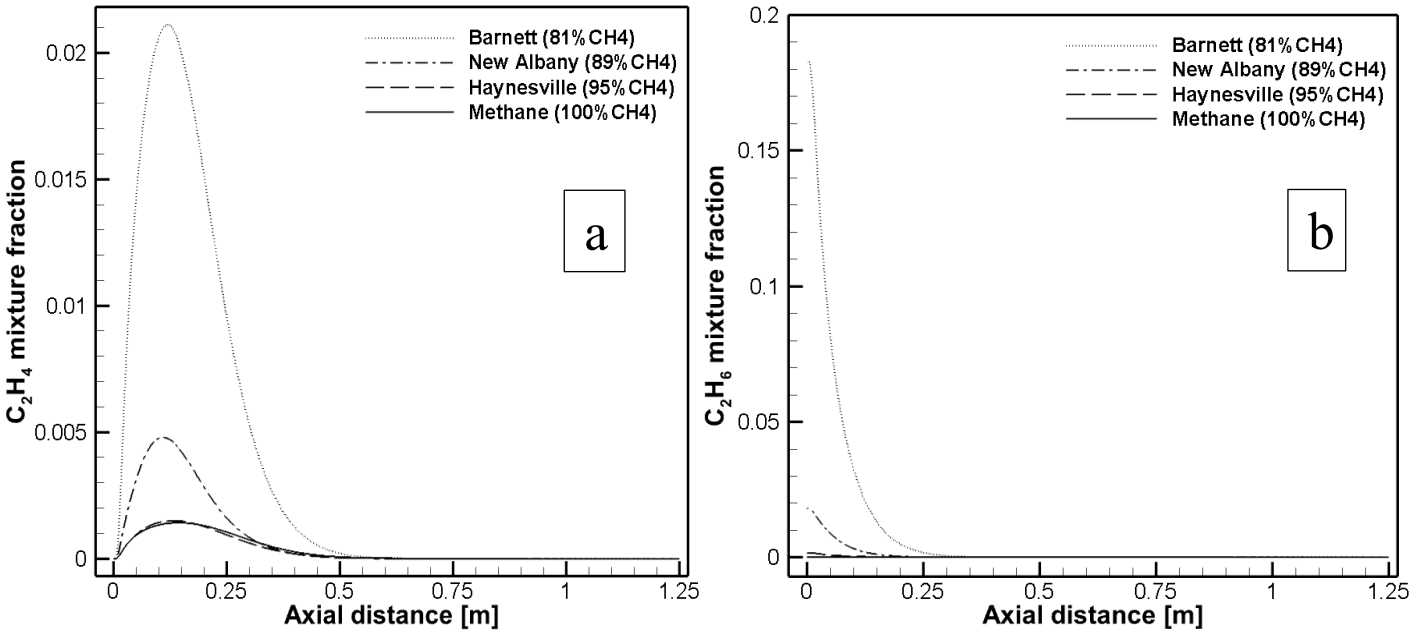

Fig. 5. The distribution of C_2H_4, C_2H_6 species on the axial line

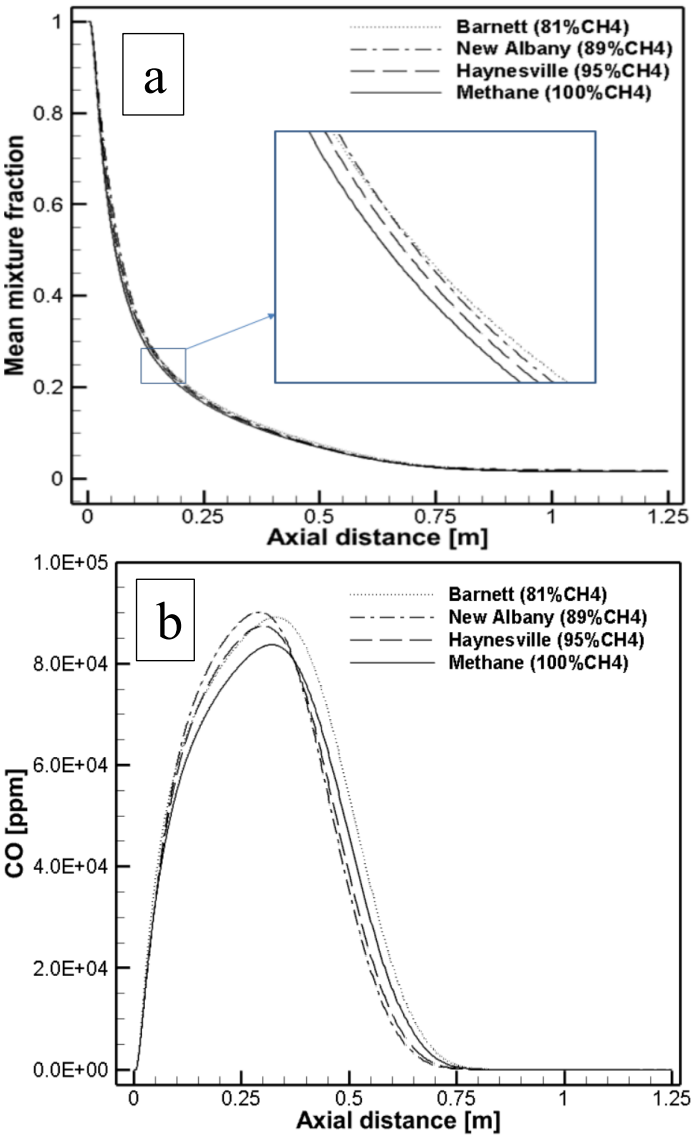

Fig. 6. Distribution of (a) mean mixture fraction and (b) CO on the axis line of the combustion chamber

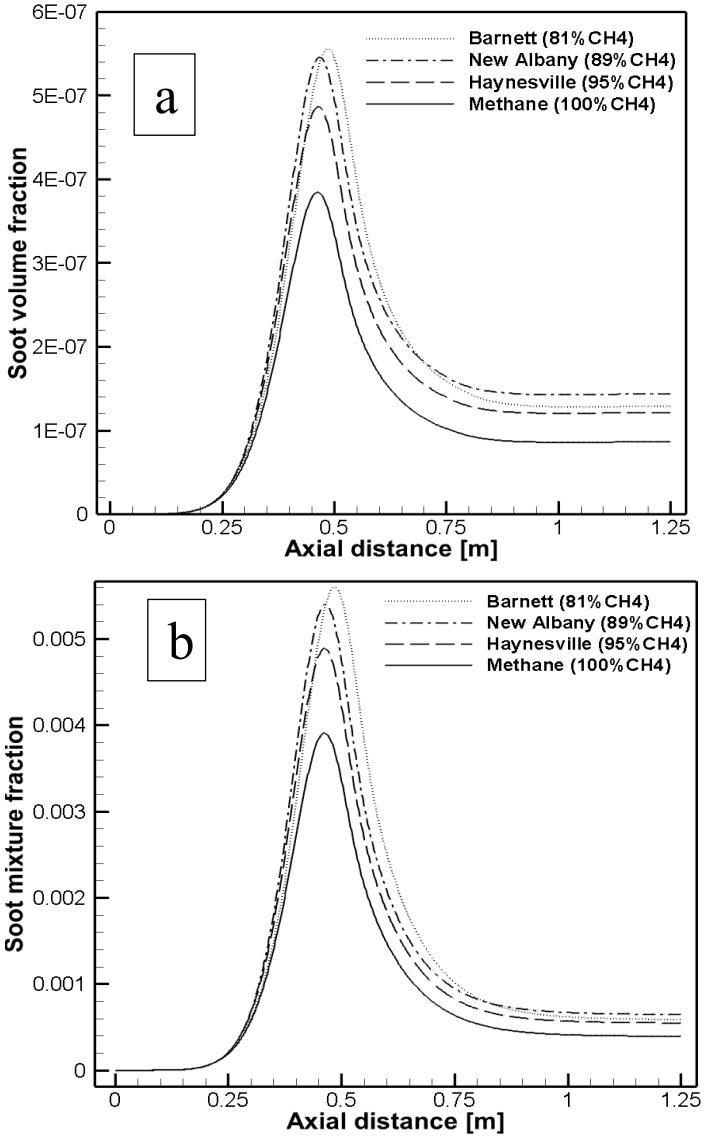

Fig. 7. The soot volume fraction distribution of shale gases on the axial line

The distributions of intermediate species such as CN, CH, and C_2H_2 released during the combustion of fuels in the combustion chamber on the axis plane are shown in Fig.8a-c. Distributions of CN and CH intermediate species in the combustion chamber are similar and it is seen that these radicals have released much more during Barnett shale gas and methane. Whereas, they are found to be less released in New Albany shale gas. The change of the C_2H_2 component in the combustion chamber during the combustion of the considered fuels is shown in Fig. 8c. In terms of C_2H_2 concentration, the highest amount is observed in Barnett shale gas, while the lowest concentration is observed during combustion of New Albany.

The distributions of flames, which result from the chemical reactions between gases and air in the combustion chamber, are shown in Fig. 9a. The flames of Barnett shale gas and methane gases are slightly longer, while the flames of New Albany and Haynesville gases are relatively short. Other properties such as flame diameters, flame temperatures, and reaction zones are approximately similar. When oxygen distributions are examined in Fig. 9b, a large amount of oxygen is seen from the entrance, and the oxygen concentration decreases towards the exit of the combustion chamber. On the other hand, the concentration is minimal in the reaction zone.

The distributions of the pollutant soot formed on the axis plane of the combustion chamber according to the fuels used are shown in Fig. 9c. In the investigations, it has been determined that the highest amount of soot is formed during the combustion of Barnett shale gas, however, the highest soot is seen in New Albany fuel at the end of the combustion chamber. The amount of soot formed during methane combustion of methane is minimal. Moreover, it has been determined that the location where the flame temperature is maximum (0.4-0.6m) is also the region where soot is maximum. Furthermore, it has determined that the axial region (0.4-0.6 m) where OH, CN, and CH intermediates species peak is also the region where the soot is maximum. On the other hand, it has been determined that the formation of soot is minimal in the entrance area of the combustion chamber where the reaction is developing gradually.

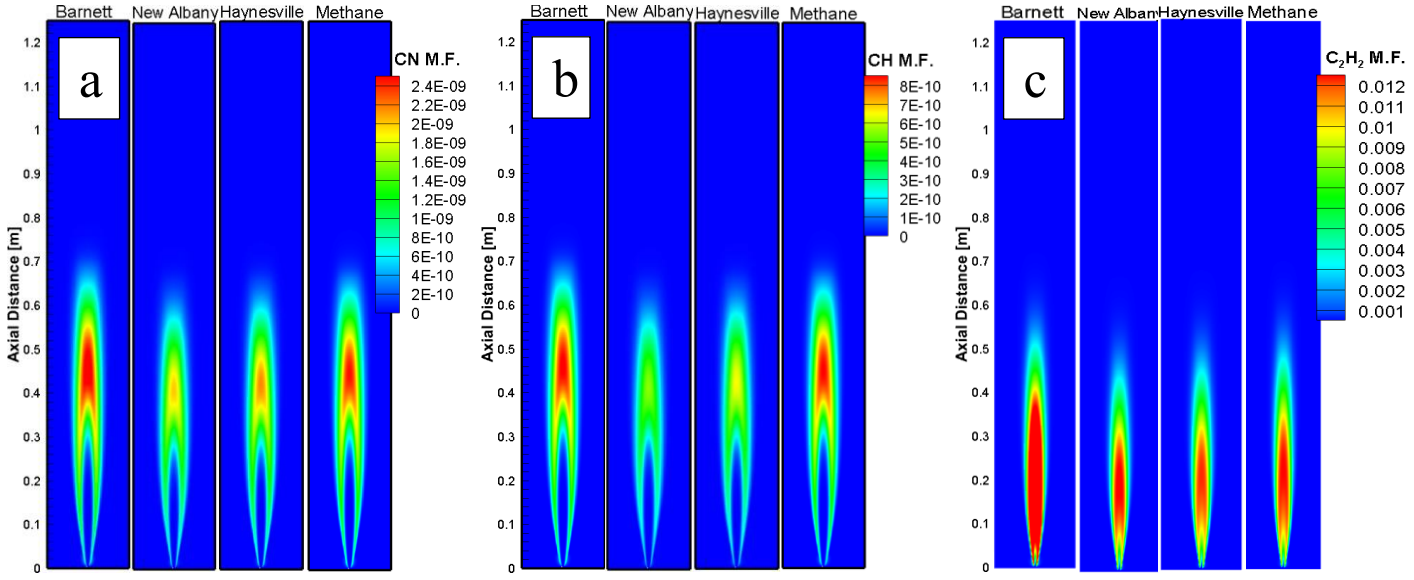

Fig. 8. Mass fraction distribution of intermediates species such as (a) CN, (b) CH, and (c) C_2H_2

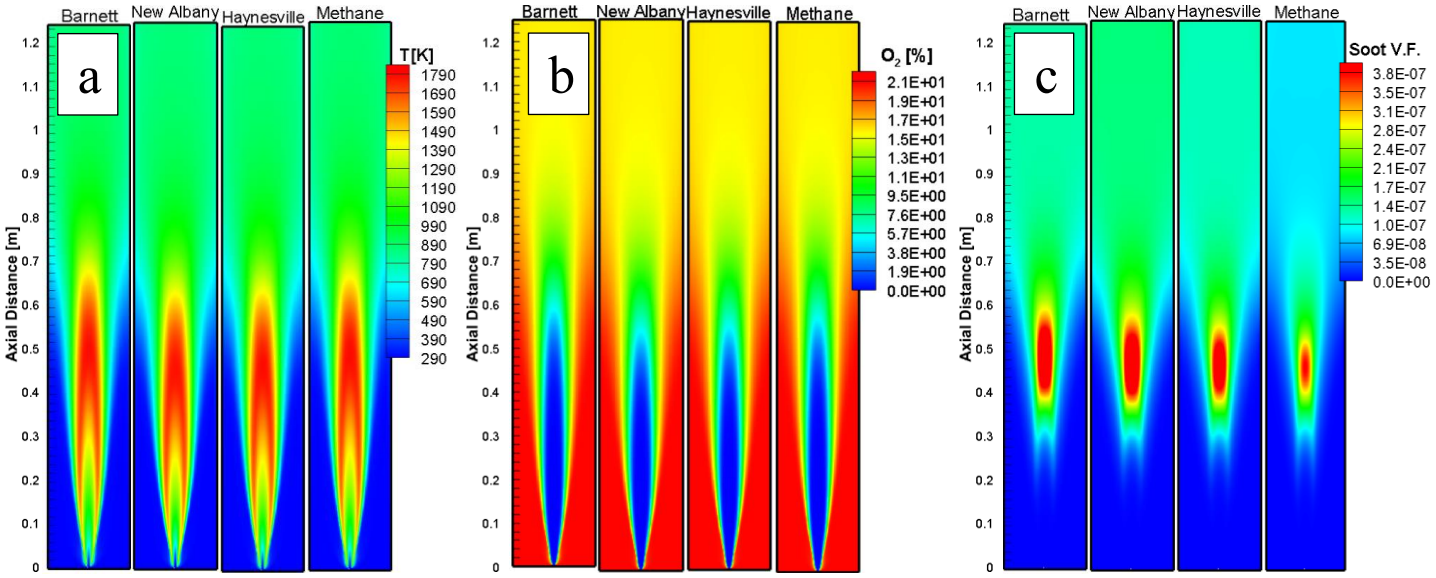

Fig. 9. (a) Flame temperatures (b), mass fraction of O_2, and (c) soot volume fraction distribution

4. Conclusions and Recommendations

In this numerical study focusing on shale gases, which have been used in the last decade and whose production amount has gradually increased, the competence of soot models have been compared with experimental data published in the literature based on methane combustion. Subsequently, the combustion and soot formation behavior of shale and methane gases have been investigated. The highlights of the study are summarized below:

- Moss-Brookes soot model predicts more accurate soot estimation than both One-Step and Method of Moments models considering the methane combustion while compared to experimental results. Moreover, One-Step estimates lower, while the Method of Moments predicts higher.
- It has been determined that the highest amount of soot is released during the combustion of Barnett shale gas whereas, it is minimal for methane.
- Although methane emits as much intermediate species as shale gases, it emits less soot than others. The reason for this situation is due to the fact that there are more unburned C elements during the combustion of shale gases. This situation is clearly understood from the graphs of CO and mean mixture fraction distribution.
- When the H/C ratio in hydrocarbon fuels increases, the formation of soot decreases or vice versa.
- In regions where the flame temperatures are maximum (0.4-0.6m) and OH, CN, and CH intermediate species reach their peak, the amount of soot for each fuel reaches its maximum levels.
- Although the flame shape of each gas is similar, it is seen that the Barnett shale gas and methane flames are longer, while the New Albany and Haynesville are relatively shorter.

5. Acknowledge

The author is grateful for the use of the computing resources provided by the National Center for High Performance Computing of Turkey (UHEM, UYBHM) under grant number 1008202020.

References

Stevens, P. (2012). The 'Shale Gas Revolution': Developments and Changes. Chatham House, 11.11.2020.

Ozturk, S. (2019). The Effect of Temperature on the Emissions of Shale Gas Combustion in USA, European Journal of Science and Technology, 16, 186-193.

EIA U.S. Energy Information Administration, (2015). Technically Recoverable Shale Oil and Shale Gas Resources: Turkey, 19.12.2020.

İlbas, M. (2017). Türkiyen'nin "Kaya Gazı" Potansiyeli, https://www.tespam.org/turkiyennin-kaya-gazi-potansiyeli/, 19.12.2020.

Karsli, S. (2015). Son Gelişmeler Işığında Türkiye'de Kaya Gazı, Iğdır Üni. Fen Bilimleri Enst. Der. / Iğdır Univ. J. Inst. Sci. & Tech. 5(3): 25-31.

Bullin K.A. and Krouskop P.E., (2008). Composition variety complicates processing plans for US shale gas, E-book, Based on: Annual Forum, Gas Processors Association, Houston Chapter, Houston, Oct. 7.

Mansurov, Z. A. (2005). Soot Formation in Combustion Processes (Review), Combustion. Explosion and Shock Waves, 41(6),727-744.

Haynes, B.S. and Wagner, H, GG., (1981). Soot Formation, Prog. Energy Combust. Sci., 7, 229-273.

Environmental Defence Fund (EDF), (t.y). Health impacts of air pollution, https://www.edf.org/health/health-impacts-air-pollution, 11.11.2020.

Gheorghe, I. F., and Ion B. (2011). The Effects of Air Pollutants on Vegetation and the Role of Vegetation in Reducing Atmospheric Pollution, The Impact of Air Pollution on Health, Economy, Environment and Agricultural Sources, Dr. Mohamed Khallaf (Ed.), ISBN: 978-953-307-528-0, InTech.

Gurbuz, H. and Sandalci T. (2019). Investigation of Effects of Fumigation on Performance and Emission in Dual Fuel Engines Injection-Controlled With Electronic Card, 5(3), 24-31.

Gurbuz, H. (2020). Analysis of the effects of multiple injection strategies with hydrogen on engine performance and emissions in diesel engine, 45, 27969-27978.

AEA (Compiled by Daniel Forster and Jonathan Perks), (2012). Climate impact of potential shale gas production in the EU Final Report, Report for European Commission DG CLIMA, Ref: ED57412- Issue 1, AEA/R/ED57412.

Vargas, A.C. Arrieta, A.A. and Arrieta, C.E. (2016). Combustion characteristics of several typical shale gas mixtures, Journal of Natural Gas Science and Engineering, 33, 296-304.

Lu, J., Ren, X., and Cao, L., (2016). Studies on Characteristics and Formation of Soot Nanoparticles in an Ethylene/Air Inverse Diffusion Flame Journal of Energy Engineering, 142(3), 04015041-1:8.

Cuoci, A., Frassoldati, A., Faravelli, T., and Ranzi, E., (2008). Kinetic Modeling of Soot Formation in Turbulent Nonpremixed Flames, Environmental Engineering Science, 25, 1407-1422.

Razak, M.F.A., Salehi, F., and Chishty, M.A., (2019). An Analysis of Turbulent Mixing Effects on the Soot Formation in High Pressure n-dodecane Sprays, Flow, Turbulence and Combustion, 103, 605-624.

Hernandez, I., Lecocq, G., Poitou, D., Riber, E., and Cuenot, B., (2013). Computations of soot formation in ethylene/air counterflow diffusion flames and its interaction with radiation, Comptes Rendus Mécanique, 341(1-2), 238-246.

Watanabe, H., Kurose, R., Komori, S., Pitsch, H., (2006). A numerical simulation of soot formation in spray flames, Center for Turbulence Research Proceedings of the Summer Program, 325-336.

Manin, J, Skeen, S, Pickett, L, Kurtz, E. et al., (2014). Effects of Oxygenated Fuels on Combustion and Soot Formation/Oxidation Processes, SAE Int. J. Fuels Lubr. 7(3):704-717.

Lautenberger C.W., de Ris, J.L., Dembsey, N.A., Barnett, J.R., and Baum, H.R., (2005). A simplified model for soot formation and oxidation in CFD simulation of non-premixed hydrocarbon flames, Fire Safety Journal 40, 141–176.

Palazzo, N., Kögl, M., Bauer, P., Mannazhi, M.N., Zigan, L., Huber, F.J.T., and Will, S., (2019). Investigation of Soot Formation in a Novel Diesel Fuel Burner, Energies, 12 (3), 1993. https://doi.org/10.3390/en12101993.

Ito, T., Kitamura, T., Ueda, M., Matsumoto, T., Senda, J., and Fujimoto, H., (2003). Effects of Flame Lift-Off and Flame Temperature on Soot Formation in Oxygenated Fuel Sprays, Sae Technical Paper Series, 2003-01-0073.

Roditcheva, O.V., Bai, X.S., (2001). Pressure effect on soot formation in turbulent diffusion flames, Chemosphere 42, 811–821.

Xu, K., Zhang, H., Shen, W., Zhang, Y., and Wu, Y., and Lyu J, (2020). Soot Formation and Distribution in Coal Jet Flames over a Broad Range of Coal Concentration, Energy Fuels, 34, 7545-7553.

Kazem B., Mohammad, M., and Iman, Z., (2007). Studies on Soot Formation and Combustion in Turbulent Spray Flames: Modeling and Experimental Measurement, 26(3), 45-54.

Chong S.T., Raman V, Mueller M.E., Selvaraj P, Im H.G., (2019). Effect of soot model, moment method, and chemical kinetics on soot formation in a model aircraft combustor, Proceedings of the Combustion Institute, 37(1), 1065-10774.

Brookes, S. J., and Moss J.B., (1999). Measurements of Soot Production and Thermal Radiation From Confined Turbulent Jet Diffusion Flames of Methane, Combustion and Flame, 116, 49-61.

Ansys Inc, (2018). Ansys® Academic Research, Release 18.2.

Afshari, F., Zavaragh, H.G., Sahin, B., Grifoni, R.C., Corvaro, F., Marchetti, B., Polonara, F., (2018). On numerical methods; optimization of CFD solution to evaluate fluid flow around a sample object at low Re numbers, Mathematics and Computers in Simulation, 152, 51-68.

Ansys Inc., ANSYS FLUENT 12.0/12.1 Documentation, (2009). Reynolds-Averaged Approach vs. LES, https://www.afs.enea.it/project/neptunius/docs/fluent/html/th/node45.htm, 11.11.2020.

Khan I.M., Greeves G., A method for Calculating the Formation and Combustion of Soot in Diesel Engines, Heat transfer in Flames, Chapter 25. Scripta, Washington DC, 1974.

Frenklach M., and Harris, S. J. (1987). Aerosol dynamics modeling using the method of moments," Journal of Colloid And Interface Science, 118(1 252–261.

Frenklach, M., (2002). Method of moments with interpolative closure," Chemical Engineering Science, 57, 2229–2239.

Bodor A.L. (2019) Numerical modelling of soot formation and evolution in laminar flames with detailed kinetics, Chemical and Process Engineering, Université Paris-Saclay; Politecnico di Milano. English. NNT : 2019SACLC050.

Bullin K.A. and Krouskop P.E., (2008). Composition variety complicates processing plans for US shale gas, E-book,

Based on: Annual Forum, Gas Processors Association, Houston Chapter, Houston, Oct. 7.

Cellek, M.S. (2020). Turbulent flames investigation of methane and syngas fuels with the perspective of near-wall treatment models, International Journal of Hydrogen Energy, 45(60), 35223-35234.